Theoretical analysis of the self-frequency shift near zero-dispersion points: Soliton spectral tunneling

Eduard N. Tsoy* and C. Martijn de Sterke
Centre of Excellence for Ultrahigh-bandwidth Devices for Optical Systems, School of Physics, University of Sydney, Sydney, New South Wales 2006, Australia
(Received 25 June 2007; published 5 October 2007)

Soliton dynamics under the action of higher-order dispersion and the Raman effect is analyzed. Though we consider a wide variety of parameters, a particularly interesting phenomenon occurs when the presence of cubic and quartic dispersion results in two regions of anomalous group velocity dispersion (GVD) separated by a region of normal dispersion. In this case a sharp switching of the soliton frequency from one anomalous GVD region to the other may exist. During such a transformation, the center of the soliton spectrum passes through the normal GVD region. We show that this switching occurs due to the phase matching between the soliton and the resonance frequency in the two anomalous GVD regions.

DOI: 10.1103/PhysRevA.76.043804 PACS number(s): 42.65.Tg, 42.65.Re, 05.45.Yv

I. INTRODUCTION

The Raman effect plays an important role in the propagation of subpicosecond optical pulses. The effect is the scattering of a photon off an optical phonon, which usually generates a lower-frequency optical ("Stokes") wave. The growth of the Stokes wave is characterized by the Raman gain coefficient. In silica glass, the bandwidth of the Raman gain [1] is up to 40 THz with a maximum near 13 THz. Therefore, for subpicosecond pulses with a relatively wide spectrum, the transfer of the energy due to the Raman effect can result in a continuous downshift of the pulse center frequency. The effect of the soliton self-frequency shift (SFS) was first observed in an optical fiber by Mitschke and Mollenauer [2]. Gordon [3] demonstrated theoretically that the rate of the SFS is approximately proportional to τ^{-4}, where τ is the pulse's temporal width. He assumed that the group velocity dispersion (GVD) does not depend on frequency and that therefore the pulse width and the SFS rate are constant with the propagation.

In many applications, such as supercontinuum generation [4,5] and frequency conversion, the dependence of the GVD on frequency is important, especially if the operating frequency is close to a zero-dispersion point (ZDP). Here we analyze how the rate of SFS changes when higher-order dispersion is taken into account. This problem is part of the general problem of the pulse dynamics near a ZDP in the presence of higher-order linear and nonlinear effects (see, e.g., Refs. [6–8] and references therein). However, in that work, the analysis was restricted mainly to including cubic dispersion (CD) [6–8].

In tapered fibers and microstructured optical fibers (MOFs), the dispersion profile can have two ZDPs. Usually, the region of anomalous GVD is located between the two normal GVD regions. For some designs of MOFs (see, e.g., [9–13] and references therein) and for an appropriate choice of materials of tapered fibers, the complementary dispersion profile can be realized. Namely, in some wavelength interval, the normal GVD region can be between the two anomalous GVD regions. Both these cases of the GVD profile can be modeled by adding cubic and quartic dispersion (QD) terms. Therefore, in the present work we ignore dispersion terms higher than quartic. When dispersion has two (or more) anomalous GVD regions separated by a normal one, it is possible that a pulse spectrum switches sharply from the one anomalous region to the other upon propagation [13,14].

The aim of the present paper is twofold. First, the physical mechanism of the switching, which is a manifestation of soliton spectral tunneling [13,14], is ascertained (see Secs. III B and IV B 3). Second, we intend to identify different types of the pulse dynamics depending on CD and QD values.

The paper is organized as follows. In Sec. II, the basic model, which includes CD, QD, and the Raman effect, is presented. Also, approximate equations for the adiabatic soliton dynamics are derived. The properties of linear waves are discussed in Sec. III A. The soliton dynamics is described by using the perturbation theory and numerical modeling in Sec. IV. A summary of different regimes and conclusions are presented in Sec. V.

II. MODEL AND APPROXIMATE EQUATIONS

The propagation of pulses in optical fibers is described by the generalized nonlinear Schrödinger equation (NLSE)

$$i\frac{\partial\psi}{\partial z} - \frac{\bar{\beta}_2}{2}\frac{\partial^2\psi}{\partial t^2} + \gamma|\psi|^2\psi = \frac{i\bar{\beta}_3}{6}\frac{\partial^3\psi}{\partial t^3} - \frac{\bar{\beta}_4}{24}\frac{\partial^4\psi}{\partial t^4} + \gamma T_R\psi\frac{\partial|\psi|^2}{\partial t}. \tag{1}$$

Here $\psi(t,z)$ is the slowly varying envelope of the field at the reference frequency $\bar{\Omega}$, z is the propagation distance, and $t=t'-z/v_g$ is the retarded time, where t' is the real time and v_g is the group velocity at $\bar{\Omega}$. The parameters $\bar{\beta}_k$, $k=2,3,4$ are the dispersion coefficients at the reference frequency, which is indicated by the overbar. The β parameters without the overbar denote the functional dependences of the disper-

*Also at the Physical-Technical Institute of the Uzbek Academy of Sciences, Tashkent-84, Uzbekistan.

sion characteristics on frequency and are defined in Sec. III A. The Kerr nonlinear coefficient γ is taken to be positive. T_R is the characteristic time scale of the Raman scattering. We use a simplified description of the Raman effect that is justified for pulses $\gtrsim$50 fs. We also ignore self-steepening [15] which is an appropriate assumption for this type of pulses.

The soliton solution of the unperturbed NLSE (1) with $\bar{\beta}_3=\bar{\beta}_4=T_R=0$ is

$$\psi_s(t,z)=\sqrt{P_s}\,\mathrm{sech}\left(\frac{t-\kappa z}{\tau}\right)\exp\left[-i\omega_s t+\frac{i}{2}(\gamma P_s+\omega_s\kappa)z\right], \tag{2}$$

where $P_s=|\bar{\beta}_2|/(\gamma\tau^2)$ is the soliton peak power, $\kappa=\bar{\beta}_2\omega_s$, and the pulse width τ and the center frequency ω_s are free parameters.

For the description of the adiabatic soliton dynamics, we use a trial function close to the solution (2):

$$\psi(t,z)=A\,\mathrm{sech}\left(\frac{t-t_c}{\tau}\right)\exp\{i[-\omega_s(t-t_c)+\mu(t-t_c)^2]\}, \tag{3}$$

where the amplitude A, the position of the pulse maximum t_c, and the chirp parameter μ, τ, and ω_s are free parameters that change on z.

The perturbation equations, found from the method of moments [16] (see also the Appendix), for the soliton parameters are

$$\frac{dQ}{dz}\equiv\frac{d(2A^2\tau)}{dz}=0, \tag{4}$$

$$\frac{d\omega_s}{dz}=-\frac{4Q\gamma T_R}{15\tau^3}, \tag{5}$$

$$\frac{d\tau}{dz}=-2\hat{\beta}_2\mu\tau-\hat{\beta}_4\left[\frac{7}{15}\pi^2\mu^3\tau^3+\frac{(\pi^2-6)}{3\pi^2}\frac{\mu}{\tau}\right], \tag{6}$$

$$\frac{d\mu}{dz}=\frac{1}{\pi^2\tau^4}[2\hat{\beta}_2(\pi^2\mu^2\tau^4-1)-\gamma Q\tau]+\frac{7\hat{\beta}_4}{15\pi^2\tau^6}(\pi^4\mu^4\tau^8-1), \tag{7}$$

$$\frac{dt_c}{dz}=\hat{\beta}_1+\frac{\hat{\beta}_3}{6\tau^2}(\pi^2\mu^2\tau^4+1). \tag{8}$$

The hat sign above the β parameters indicates that a value is found at the soliton frequency ω_s—i.e., $\hat{\beta}_k=\beta_k(\omega_s)$, $k=1,\ldots,4$. Since we include higher-order dispersion up to $\bar{\beta}_4$ only [see Eq. (1)], $\hat{\beta}_4=\bar{\beta}_4$ (see Sec. III A). As follows from Eq. (4) the pulse total energy Q is constant; therefore, the evolution of amplitude A can be found from that of τ. We note that the invariance of Q is due to the truncated response of the Raman effect and the neglect of losses.

During the propagation, the soliton changes its parameters and also emits linear waves, or radiation. A method for the full treatment of radiation including a calculation of its amplitude is presented, for example, in Ref. [7]. However, in many cases the amount of energy transferred to the radiation is small, compared with that in the soliton, and therefore the soliton dynamics is affected only slightly. The situation may change considerably when soliton transfer energy to a resonance frequency discussed in the next Sec. III A.

III. LINEAR WAVES

A. Dispersion relation

We mainly study the soliton dynamics, and therefore we do not include explicitly radiation. However, it is important for the following discussion to analyze the parameters of linear waves. The dispersion relation (in the retarded reference frame) of linear waves, as found from Eq. (1) with $\gamma=0$, is

$$\beta(\omega)=\frac{\bar{\beta}_2}{2}\omega^2+\frac{\bar{\beta}_3}{6}\omega^3+\frac{\bar{\beta}_4}{24}\omega^4, \tag{9}$$

where $\beta(\omega)$ is the propagation constant and $\omega=\Omega-\bar{\Omega}$ is the difference between the (actual) frequency Ω and the reference frequency $\bar{\Omega}$. In the retarded frame, there is always an extremum of the dispersion relation at $\omega=\omega_{e1}=0$. The other extremum frequencies $\omega_{e2,e3}$ are found from

$$\omega_{e2,e3}=\frac{3}{2\bar{\beta}_4}(-\bar{\beta}_3\pm\sqrt{D_e}),\quad D_e=\bar{\beta}_3^2-\frac{8}{3}\bar{\beta}_2\bar{\beta}_4. \tag{10}$$

The functional dependence of the group velocity (in the retarded reference frame) $\beta_1(\omega)$, GVD $\beta_2(\omega)$, and CD $\beta_3(\omega)$ on ω are found from Eq. (9) as $\beta_k(\omega)=\partial^k\beta(\omega)/\partial\omega^k$, $k=1,2,3$, or explicitly for the GVD,

$$\beta_2(\omega)=\bar{\beta}_2+\bar{\beta}_3\omega+\frac{\bar{\beta}_4}{2}\omega^2. \tag{11}$$

The ZDPs $\omega_{p1,p2}$ are given by

$$\omega_{p1,p2}=\frac{1}{\bar{\beta}_4}(-\bar{\beta}_3\pm\sqrt{D_p}),\quad D_p=\bar{\beta}_3^2-2\bar{\beta}_2\bar{\beta}_4. \tag{12}$$

The $(\bar{\beta}_3,\bar{\beta}_4)$ plane has eight regions with different behavior of the dispersion relation and GVD. This is summarized in Fig. 1, where $\bar{\beta}_2<0$ is taken. Figure 1 and other figures in the paper represent values in dimensionless units. The solid and dashed lines in Fig. 1 correspond to $D_e=0$ and $D_p=0$, respectively. There are two ZDPs and three extrema of $\beta(\omega)$ in regions 1, 2, 5, and 6, two ZDPs and one extremum of $\beta(\omega)$ in regions 3 and 7, and no ZDPs and one extremum of $\beta(\omega)$ in regions 4 and 8 of the figure. Typical examples of the dispersion relation (in the retarded reference frame) and GVD for $\bar{\beta}_3<0$ are presented in Fig. 2. The corresponding curves for $\bar{\beta}_3>0$ (region 5–8 in Fig. 1) are obtained by reflection about $\omega=0$. The different dispersion relations give rise to different dynamics of the soliton under the Raman shift, as demonstrated in Sec. IV.

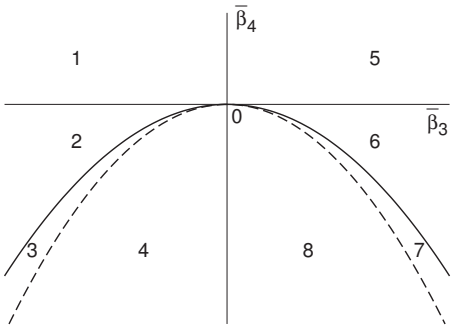

FIG. 1. Regions in the $(\bar{\beta}_3, \bar{\beta}_4)$ plane with different behavior of the dispersion relation and GVD. The solid and dashed lines are $D_e=0$ and $D_p=0$ in Eqs. (10) and (12), respectively.

B. Phase-matching frequency

The frequency of the radiation, emitted by the soliton in the presence of higher-order effects, can be found from a "phase-matching" argument [17]. The Fourier transform of Eq. (2) shows that the soliton can be represented as a superposition of plane waves of the form $\exp\{i(\eta(\omega)z-\omega t)\}$, where

$$\eta(\omega) = \frac{\gamma}{2}P_s + \beta(\omega_s) + (\omega-\omega_s)\beta_1(\omega_s). \tag{13}$$

Here we use $\omega_s\kappa/2 \approx \beta(\omega_s)$ and $\kappa = d\beta(\omega_s)/d\omega_s \equiv \beta_1(\omega_s)$ [7,17]. Equation (13) can be considered as the "soliton dispersion relation," and $\eta(\omega)$ can be regarded as the soliton propagation constant. The function $\eta(\omega)$ is a straight line that is parallel to the tangent of $\beta(\omega)$ at $\omega=\omega_s$ and shifted up by a value $\gamma P_s/2$. The phase matching requires the equality of the soliton and radiation propagation constants; therefore, the resonance frequency ω_r is found from [7,17]

$$\eta(\omega_r) = \beta(\omega_r). \tag{14}$$

The amplitude of radiation depends on the amplitude of the soliton spectrum at $\omega=\omega_r$. The closer is ω_r to ω_s, the larger is the amplitude of the radiation.

When ω_r is in a normal GVD region, then linear waves (radiation) are excited. This is a common case, and it is widely used in the interpretation of supercontinuum (SC) generation experiments [5]. This regime is shown in Fig. 3(a). The soliton propagation constant $\eta(\omega)$ (dotted line) is parallel to $\beta(\omega)$ (solid line) at ω_s (solid circle). The dashed line represents the GVD $\beta_2(\omega)$. The intersection of the dotted and solid lines solves Eq. (14), giving the phase-matched frequency ω_r (the open circle) in the normal GVD region.

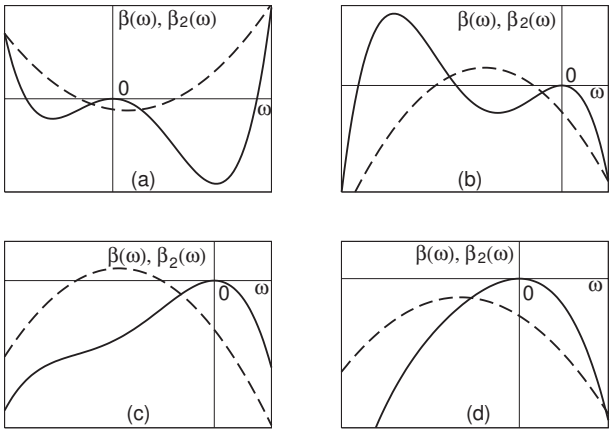

FIG. 2. Typical examples of dispersion relation (9) (solid line) and GVD (11) (dashed line) for different values of $\bar{\beta}_3$ and $\bar{\beta}_4$. Cases (a), (b), (c), and (d) correspond to regions 1, 2, 3, and 4 in Fig. 1, respectively.

For some $\bar{\beta}_3$ and $\bar{\beta}_4$, such as in Figs. 2(b) and 2(c), the resonance frequency can occur in the anomalous GVD region; see Fig. 3(b). Since GVD at ω_r is such that solitons can exist, the energy of the initial soliton is transferred not only to linear waves, but can form a soliton at the resonance frequency. This process is revealed as a sharp switching of the soliton frequency from the one anomalous GVD region to the other. During such switching the soliton spectrum passes through the normal GVD region. This *spectral tunneling* effect was observed numerically by Serkin *et al.* [14]. Recently, the possibility of such a process in MOFs was studied by Kibler *et al.* [13]. However, the physical mechanism of the spectral tunneling was not discussed in Refs. [13,14]. Here, we emphasize that spectral tunneling occurs due to the phase matching between the soliton frequency ω_s and the resonance frequency ω_r, being in different anomalous GVD regions. We consider this effect in more detail in Sec. IV B 3.

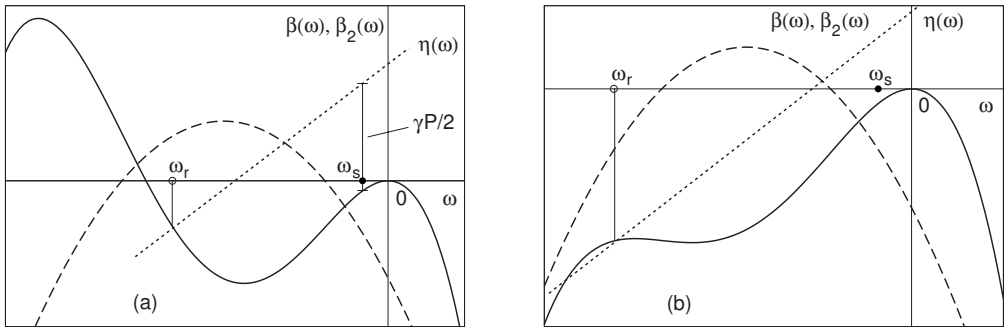

FIG. 3. A graphical solution of Eq. (14) for the phase-matched frequency. The solid, dashed, and dotted lines correspond to $\beta(\omega)$, $\beta_2(\omega)$, and $\eta(\omega)$, respectively. The soliton frequency ω_s (resonant frequency ω_r) is indicated by a solid (open) circle. (a) ω_r is in the normal GVD region, and (b) ω_r is in the anomalous GVD region.

IV. SOLITON DYNAMICS

The soliton dynamics depends on the relative position of $\omega_s(0)$ with respect to the ZDPs. Since the soliton frequency is shifted down, the ZDPs that are approached become increasingly important, compared to the ZDPs from which the spectrum moves away. Below, if not stated otherwise, we assume that the reference frequency $\bar{\Omega}$ coincides with the carrier (laser) frequency—i.e., $\omega_s(0)=0$.

In the next sections we analyze the dynamics for different sets of the parameters. The analysis is based on the perturbation equations (4)–(8), the phase-matching condition (14), and the direct numerical simulation of Eq. (1). The key effects, including the spectral tunneling, which require quartic or higher-order dispersion, are described in Sec. IV B 3.

A. Case $T_R=0$

In this case, Eq. (5) shows that the soliton center frequency does not change with z. Then Eqs. (6) and (7) have several fixed points (FPs) with a stable fixed point corresponding to a stable soliton if we ignore the loss of energy by the soliton to radiation. Equations (6) and (7) have FPs with $\mu=0$ and $\mu\neq 0$. We consider only stationary states with $\mu=0$, assuming that the initial pulse has no chirp.

The FPs at $\mu=0$ are found from Eq. (7) with $d\mu/dz=0$:

$$\tau^3+\frac{2\hat{\beta}_2}{\gamma Q}\tau^2+\frac{7\hat{\beta}_4}{15\gamma Q}=0. \tag{15}$$

There are three different cases for $\mu=0$: (i) when $\hat{\beta}_4>0$ and $\hat{\beta}_2$ and $\hat{\beta}_4$ satisfy the condition

$$\frac{\hat{\beta}_2^3}{\hat{\beta}_4\gamma^2Q^2}<-\frac{63}{160}\approx -0.394, \tag{16}$$

there are two positive roots, corresponding to one stable and one unstable FP, for τ; (ii) when $\hat{\beta}_4>0$ and condition (16) is not satisfied, there are no roots with $\tau>0$; (iii) when $\hat{\beta}_4<0$, there is one root (a stable FP) with $\tau>0$. If Eqs. (6) and (7) have a stable FP, $(\tau,\mu)=(\tau_F,0)$, then $\tau\to\tau_F$ as $z\to\infty$. If Eqs. (6) and (7) have no stable FPs, then $\tau\to\infty$ as $z\to\infty$ so that the soliton disappears, becoming wider and lower in amplitude.

For small $\hat{\beta}_4$, one can write an approximate solution of Eq. (15):

$$\tau\approx\tau_u\left(1+\frac{7}{120}\frac{\hat{\beta}_4\gamma^2Q^2}{\hat{\beta}_2^3}\right),\quad \tau_u=-\frac{2\hat{\beta}_2}{\gamma Q}, \tag{17}$$

where τ_u is the soliton width of the unperturbed NLSE with the dispersion coefficient $\hat{\beta}_2$. This solution becomes invalid close to a ZDP.

B. General case $T_R\neq 0$

It is well known [2,3] [see also Eq. (5)] that the Raman effect shifts the soliton center frequency ω_s. However, if $T_R\ll\tau$, one can still use the behavior described in Sec. IV A, assuming adiabatic variation of $\hat{\beta}_2$ and $\hat{\beta}_3$ on z. This variation corresponds qualitatively to the variation of $\hat{\beta}_2$ point along the GVD curve (see Fig. 2) to lower frequencies. The change of $\hat{\beta}_2$ also means that the type of soliton dynamics, described in Sec. IV A, can vary upon propagation.

In all numerical simulations of Eq. (1) and corresponding plots, we use dimensionless units, taking $\bar{\beta}_2=-1$ and $\gamma=1$. The initial condition was taken in the form of the soliton with $\tau(0)=A(0)=1$ and $\omega_s(0)=\mu(0)=0$.

1. $\bar{\beta}_3\neq 0$ and $\bar{\beta}_4=0$

This case, in which $\beta_2(\omega)$ varies linearly with frequency, was considered in detail in Refs. [6–8]. It was shown that for $\bar{\beta}_3>0$, the SFS is slower than that at $\bar{\beta}_3=0$ where the dependence of ω_s on z is linear [3]. The qualitative explanation is that the Raman effect shifts the soliton spectrum away from the ZDP, so that $|\hat{\beta}_2|$ and the soliton width increase [see Eq. (17)], resulting in a deceleration of the frequency shift [see Eq. (5)]. For $\bar{\beta}_3<0$, the Raman effect shifts the soliton spectrum towards the ZDP, $|\hat{\beta}_2|$ and τ decrease [see Eq. (17)], and the SFS rate initially speeds up. When the soliton spectrum is close to the ZDP, the energy effectively transfers to the resonant radiation in the normal dispersion region. This process, which was observed experimentally [6], suppresses the further soliton SFS [6,7].

In Ref. [8], explicit expressions for the soliton frequency and the pulse width were obtained. We write the expressions here for completeness (note also that the soliton frequency defined in Ref. [8] has opposite sign than ω_s used here):

$$\omega_s=-\frac{1}{\bar{\beta}_3}\left[\bar{\beta}_2+\left(\hat{\beta}_{2,0}^4+\frac{2}{15}\bar{\beta}_3T_R\gamma^4Q^4z\right)^{1/4}\right],$$

$$\tau\approx -2\hat{\beta}_2/(\gamma Q), \tag{18}$$

where $\hat{\beta}_{2,0}=\hat{\beta}_2(z=0)$. For $\bar{\beta}_3<0$, Eqs. (18) are valid for $z<z_{th}$, where

$$z_{th}=-\frac{15}{2}\frac{\hat{\beta}_{2,0}^4}{\bar{\beta}_3T_R\gamma^4Q^4}. \tag{19}$$

The threshold length z_{th} defines the propagation distance over which the soliton approaches the ZDP and transfers the energy to radiation. The frequency of the radiation can be found from the phase-matching condition (14). As a rough estimate of ω_s at which the effective transfer of energy occurs, one can take the ZDP frequency.

The suppression of the SFS discussed above occurs for moderate values of T_R. We have found in numerical simulations that for fixed $\bar{\beta}_3$, when T_R/τ exceeds a threshold, the amount of energy transferred from the soliton to radiation becomes large. The energy remaining in the pulse is not enough to support the soliton, so the pulse disperses upon the propagation.

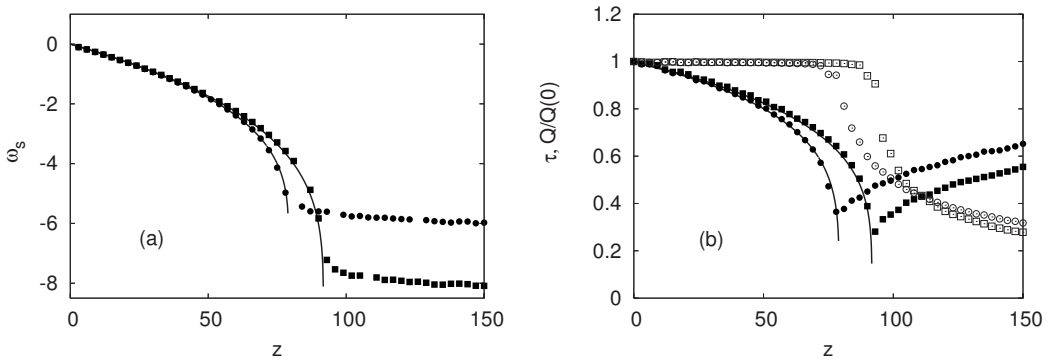

FIG. 4. Evolution for $\bar{\beta}_3<0$ and $\bar{\beta}_4>0$ of (a) the soliton frequency ω_s and (b) the width τ (solid symbols) and soliton energy Q (open symbols). Points are from numerical simulations of Eq. (1); solid lines are the solutions of Eqs. (5)–(7). Parameters are $T_R=0.05$, $\bar{\beta}_3=-0.1$, $\bar{\beta}_4=0.001$ (circles), and $\bar{\beta}_4=0.01$ (squares).

2. $\bar{\beta}_3<0$ and $\bar{\beta}_4>0$

As mentioned in Sec. I, this case is typical for many types of MOFs in a wide range of frequencies. The GVD has two ZDPs $\omega_{p1}<0$ and $\omega_{p2}>0$ [see Fig. 2(a)] such that the two normal GVD regions are separated by an anomalous one. Since the soliton frequency decreases due to the Raman effect, the influence of the ZDP ω_{p2} becomes smaller and smaller. Therefore, the dynamics is similar to that for $\bar{\beta}_4=0$ (see Sec. IV B 1).

The dependence of the soliton parameters found from numerical simulations of Eq. (1) (points) and of Eqs. (5)–(7) (lines) is shown in Fig. 4. The parameter $Q\equiv 2A^2\tau$ corresponds to the *soliton* energy. As seen from Fig. 4, a sharp decrease of ω_s and τ, occurring when the soliton spectrum approaches the ZDP ω_{p1}, is accompanied by a reduction of the soliton energy. The adiabatic approach fails after this point because it does not include any transfer of energy to radiation. However, the theory provides the correct description of the initial stage of the process. Equations (5)–(7) give also a good estimate of the threshold distance for the suppression of the Raman shift.

3. $\bar{\beta}_3<0$ and $\bar{\beta}_4<0$

For these ranges of $\bar{\beta}_3$ and $\bar{\beta}_4$, the interval between the ZDPs, ω_{p1} and ω_{p2}, where $\omega_{p1}<\omega_{p2}<0$, corresponds to normal dispersion, $\beta_2(\omega)>0$ [see Figs. 2(b) and 2(c)]. Such a situation can be realized for a range of frequencies in nanowires and in some MOFs [9–13].

For small $|\bar{\beta}_4|$ (the upper part of region 2 in Fig. 1), the interval between the ZDPs is wide. Therefore, the dynamics is qualitatively similar to that for $\bar{\beta}_4=0$; namely, ω_s saturates near the ZDP (ω_{p2} in this case), while the soliton width τ increases slightly after a sharp decrease. This is shown in Fig. 5 (see squares for $\bar{\beta}_4=-0.002$), where points corresponds to numerical simulations of Eq. (1) and lines are from Eqs. (5)–(7). Note that the soliton transfers more than 80% of its energy to radiation. The adiabatic approach (solid line for $\bar{\beta}_4=-0.002$) agrees well until the threshold distance.

The evolution of the field and spectrum for $\bar{\beta}_4=-0.002$ is shown in Figs. 6(a) and 6(b), respectively. In all plots in the time domain, we show the absolute value $|\psi|$ in order to see radiation more clearly, while plots in the frequency domain are for $|\psi|^2$. We use periodic boundary conditions, resulting in a wrapping effect in the time domain. As seen from Fig. 6(a), near the threshold distance z_{th} [cf. Eq. (19)], the soliton becomes narrow and a tail appears behind the soliton. This tail, which broadens during the propagation, is the resonant linear wave. The transfer of energy from the soliton to radiation is seen clearly in Fig. 6(b). Similar to the case in Sec. IV B 1, for fixed $\bar{\beta}_3$ and $\bar{\beta}_4$, the larger values of T_R/τ result in the disappearance of the soliton that transfers almost all its energy to radiation. For $\bar{\beta}_3=-0.1$ and $\bar{\beta}_4=-0.002$, the threshold value of T_R/τ is ~ 0.07

Moderate values of $|\bar{\beta}_4|$ correspond roughly to the bottom of region 2 and region 3 in Fig. 1. For $\bar{\beta}_3=-0.1$ the borders of region 3 are $\bar{\beta}_{4,th1}=-0.005$ and $\bar{\beta}_{4,th2}=-0.003\,75$. The variation of the soliton parameters for $\bar{\beta}_4=-0.004$ is shown by circles in Fig. 5. Now, the other ZDP ω_{p1} also affects the dynamics. Namely, the soliton spectral tunneling [13,14], or switching of soliton frequency from $\omega_s\sim\omega_{p2}$ to $\omega_s\sim\omega_{p1}$, can occur [see Figs. 6(c) and 6(d)]. The frequency shift is larger than the width of the normal GVD region and can exceed hundred nanometers in some MOFs [13]. After switching, the rate of SFS slows down due to an increase of $|\hat{\beta}_2|$ and, therefore, of the soliton width [see Eq. (5)].

For the parameters in Figs. 6(c) and 6(d), the soliton loses about 10% of its energy [see also plot by circles in Fig. 5(c)]. The linear waves now generated have a different origin; they are due to the four-wave mixing. Namely, near the threshold distance $z\approx 86$ for $\bar{\beta}_4=-0.004$, the soliton spectrum "switches" from ω_{p2} to ω_{p1} [see Fig. 6(d)]. The main part of energy centered at $\sim\omega_{p2}$ acts as a pump, while a small fraction of energy transferred to $\omega\sim\omega_{p1}$ plays a role of a signal. Then linear waves (idler) can be generated in the anomalous dispersion region at $\omega\sim 2\omega_{p1}-\omega_{p2}>0$ if the additional phase-matching condition is fulfilled. These waves are seen in Fig. 6(c) as small "noisy" ripples, and they are quite different from the resonant radiation in Fig. 6(a).

The Raman effect, changing ω_s with z, "helps" to realize the phase-matching condition (14). This means that even if one starts from an inappropriate pump frequency, then the

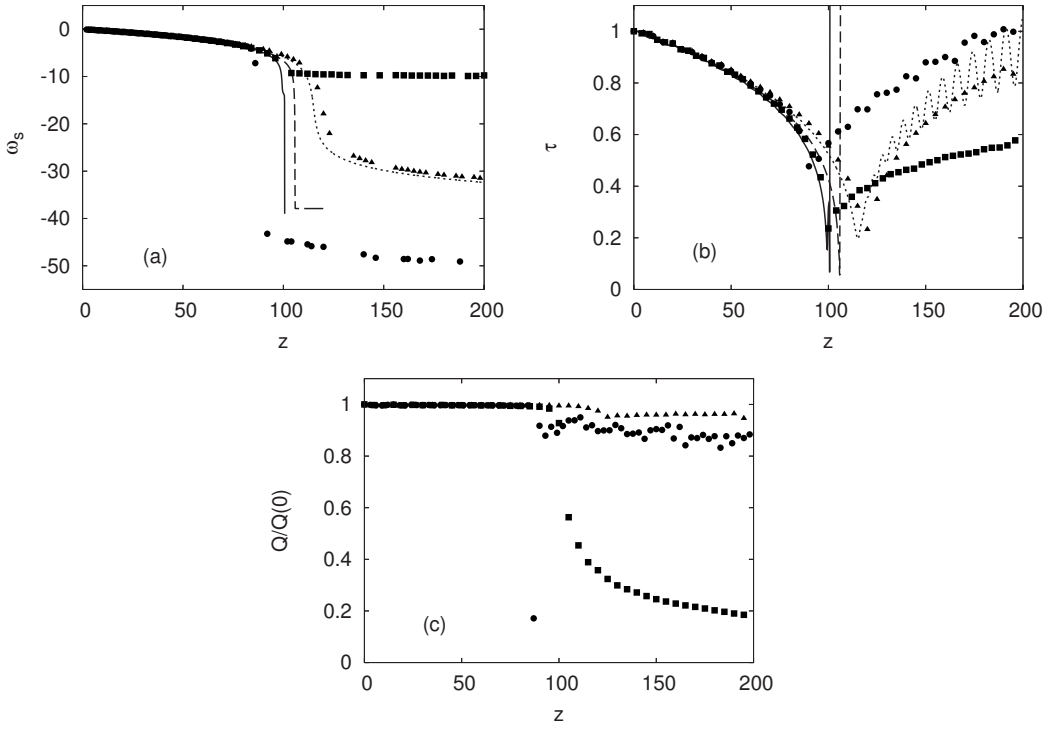

FIG. 5. Evolution for $\bar{\beta}_3<0$ and $\bar{\beta}_4<0$ of (a) the soliton frequency ω_s, (b) the width τ, and (c) soliton energy Q. Points are from numerical simulations of Eq. (1), solid lines ($\bar{\beta}_4=-0.002$), dashed lines ($\bar{\beta}_4=-0.004$), and dotted lines ($\bar{\beta}_4=-0.006$) lines for ω_s and τ are solutions of Eqs. (5)–(7). Parameters are $T_R=0.05$, $\bar{\beta}_3=-0.1$, $\bar{\beta}_4=-0.002$ (squares), $\bar{\beta}_4=-0.004$ (circles), and $\bar{\beta}_4=-0.006$ (triangles).

phase matching can be still fulfilled at some propagation distance, supposing that the solution of Eq. (14) exists. The unidirectional character of the SFS forces the energy transfer always from higher to lower frequencies.

The scenario described above for moderate $|\bar{\beta}_4|$ is one of the possible regimes. The existence of the soliton after the spectral tunneling depends on the rate of $\hat{\beta}_2$ variation determined by T_R and on a value of $\beta(\omega_r)$. The other possible regimes include the soliton breakup and appearance of multiple solitons (pulses). Figure 7 gives an example when several pulses emerge after the tunneling. The β parameters in Fig. 7 are the same as in Figs. 6(c) and 6(d), $\bar{\beta}_3=-0.1$ and $\bar{\beta}_4=-0.004$, while $T_R=0.2$ (rather then 0.05). In Fig. 7(a), there are at least three pronounced pulses that propagate with different velocities. Figure 7(b) shows that right after the tunneling, at $z\approx 20$, the energy that transferred to the other anomalous GVD region is close to the ZDP at $\omega_{p1}=-36.2$. Therefore, near that ZDP we have the variation of the spectrum reminiscent of a typical SC generation process [5]. This includes [5] the soliton fission, manifested by several peaks in anomalous GVD region near ω_{p1} in Fig. 7(b), and generation of the blueshifted waves in the normal GVD region.

For $\bar{\beta}_3$ and $\bar{\beta}_4$ in region 4 in Fig. 1, the GVD is anomalous and has one maximum and $\beta(\omega)$ has no zeros [see Fig. 2(d)]. The rate of the frequency shift speeds up when ω_s approaches the GVD maximum, and then the rate slows down when ω_s moves away from the maximum (see triangle points in Fig. 5). Since the loss of energy by the soliton is small in this case, the approximate equations (5)–(7) well describe the dynamics; see the dotted lines in Fig. 5. The soliton width follows also the variation of $\hat{\beta}_2$. Only a few percent of the soliton energy is transferred to radiation, as seen from Figs. 5(c) and 6(e). The corresponding evolution of the spectrum is shown in Fig. 6(f).

4. $\bar{\beta}_3>0$ and $\bar{\beta}_4\neq 0$

As mentioned in Sec. III A, $\beta(\omega)$ and $\beta_2(\omega)$ for $\bar{\beta}_3>0$ can be obtained from those for $\bar{\beta}_3<0$ by using the transformation $\omega\rightarrow-\omega$. Then, using the same assumption $\omega_s(0)=0$ as in Secs. IV B 1, IV B 2, and IV B 3, one can conclude that the dynamics in region 5 in Fig. 1 is similar to that in region 1 and that the dynamics in regions 6, 7, and 8 in Fig. 1 is similar to that at $\bar{\beta}_3>0$ and $\bar{\beta}_4=0$ (see Sec. IV B 1).

If $\omega_s(0)$ does not coincide with the reference frequency, then the dynamics at $\bar{\beta}_3>0$ depends on the relative positions of $\omega_s(0)$ and the ZDPs. The dynamics is qualitatively similar to that at $\bar{\beta}_3<0$ with the same relative positions of the soliton frequency and the ZDPs.

C. Estimate of parameters

Here we estimate the parameters for observation of the effects discussed above. The relations for the CD and QD parameters are

$$\bar{\beta}_k=\bar{\beta}_k^{(d)}|\bar{\beta}_2|T_0^{k-2},\quad k=3 \text{ and } 4, \tag{20}$$

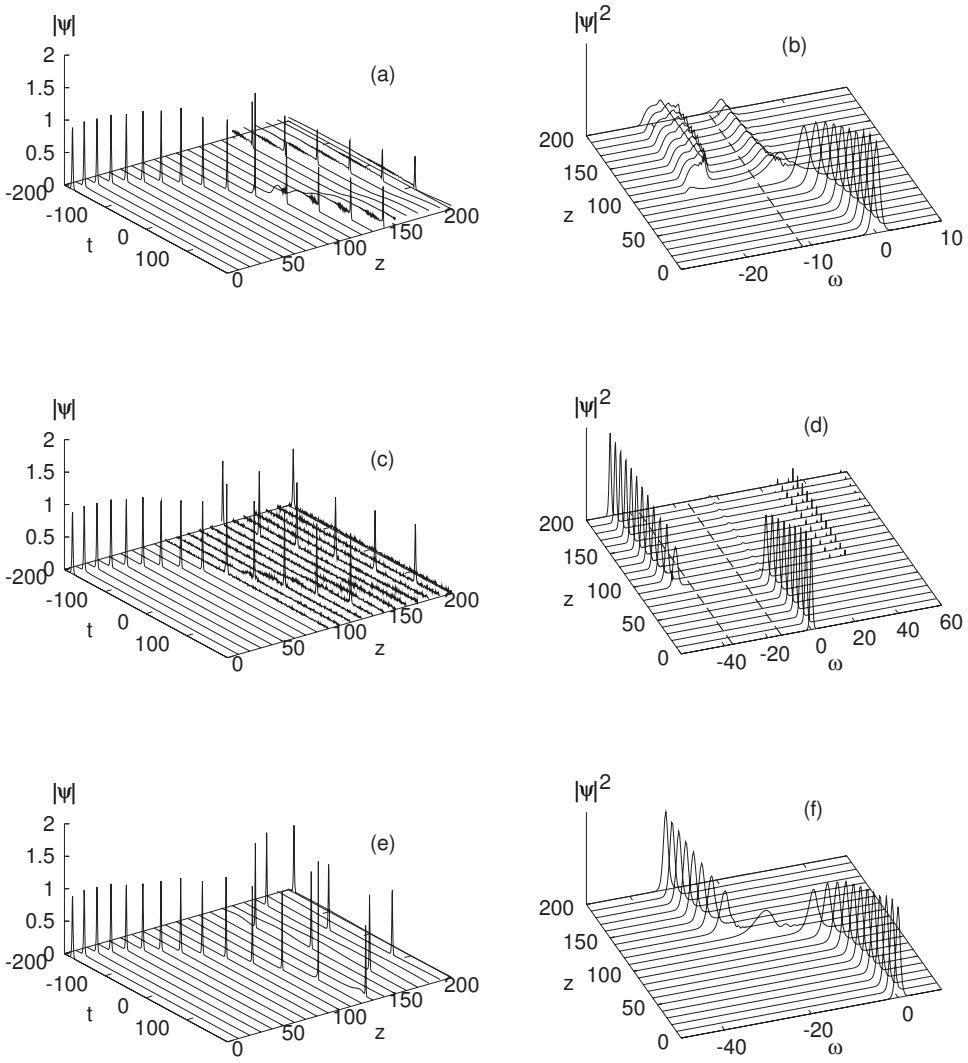

FIG. 6. Evolution of the field $|\psi(z,t)|$ [(a), (c), and (e)] and of the spectrum $|\psi(\omega,t)|^2$ [(b), (d), and (f)]. Parameters are $T_R=0.05$, $\bar{\beta}_3=-0.1$, (a) and (b) $\bar{\beta}_4=-0.002$, (c) and (d) $\bar{\beta}_4=-0.004$, and (e) and (f) $\bar{\beta}_4=-0.006$. Dashed lines in the plots of spectra show the positions of the ZDPs. The ZDP at ω_{p1} in (b) is outside the frequencies shown.

where the superscript "(d)" denotes a dimensionless parameter and T_0 is the initial pulse width. The spatial, temporal, and power characteristic scales z_{cs}, t_{cs}, and P_{cs} are defined as

$$z_{cs}=\frac{T_0^2}{|\bar{\beta}_2|},\quad t_{cs}=T_0,\quad P_{cs}=\frac{|\bar{\beta}_2|}{\gamma T_0^2}. \tag{21}$$

We take the reference wavelength $\lambda_0=1$ μm, $\bar{\beta}_2=-50$ ps^2/km, $T_0=100$ fs, and $\gamma=0.005$ (m W)$^{-1}$. Then $\bar{\beta}_3^{(d)}=-0.1$ and $\bar{\beta}_4^{(d)}=-0.004$ give $\bar{\beta}_3=-0.5$ ps^3/km and $\bar{\beta}_4=-2\times10^{-3}$ ps^4/km, respectively. For comparison, at $\lambda_0=1$ μm, the corresponding parameters are $\bar{\beta}_2\approx40$ ps^2/km, $\bar{\beta}_3\approx0.1$ ps^3/km, and $\bar{\beta}_4\approx6\times10^{-5}$ ps^4/km for SMF28 fiber and $\bar{\beta}_2\approx-50$ ps^2/km, $\bar{\beta}_3\approx0.14$ ps^3/km, and $\bar{\beta}_4\approx-2.2\times10^{-4}$ ps^4/km for an example of a MOF in Ref. [5]. Though the β parameters of SMF28 and the MOF have signs different from the required ones, the $\bar{\beta}_2$, $\bar{\beta}_3$, and $\bar{\beta}_4$ chosen have quite reasonable absolute values. It should be mentioned also that the fibers chosen for comparison are optimized for other applications.

The distance between the ZDPs [see Eq. (12)] corresponds to $\Delta\lambda=160$ nm. Therefore, the switching of the soliton frequency during the spectral tunneling is expected to be $\sim$200 nm. This requires the system length ($L^{(d)}\approx100$) $\sim$20 m and initial peak power $\sim$1 kW.

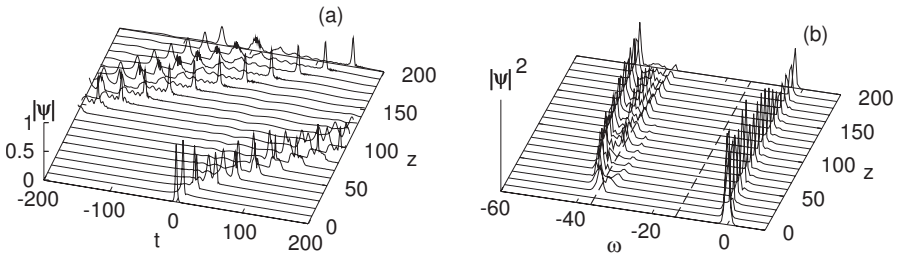

FIG. 7. Evolution of (a) the field $|\psi(z,t)|$ and (b) the spectrum $|\psi(\omega,t)|^2$. Parameters are $T_R=0.2$, $\bar{\beta}_3=-0.1$, and $\bar{\beta}_4=-0.004$. Dashed lines in the spectrum plot show the positions of the ZDPs.

V. DISCUSSION AND CONCLUSIONS

Analysis of the dynamics for various values of $\bar{\beta}_3$ and $\bar{\beta}_4$ can be summarized according to the following scenarios [recall that we take $\omega_s(0)$].

(i) $\bar{\beta}_4>0$ and $\bar{\beta}_3\lessgtr 0$ and $\bar{\beta}_4<0$ with small $|\bar{\beta}_4|$ and $\bar{\beta}_3<0$ (regions 1 and 5 and a part of region 2 in Fig. 1). For regions 1 and 5 in Fig. 1, the soliton frequency $\omega_s(0)$ is between the two ZDPs and CD at the left-hand side the ZDP frequency is negative. In region 2, both ZDPs are on the left-hand side of the soliton frequency. The CD of the nearest ZDP is also negative, while the influence of the second ZDP is negligible. In this case, the Raman SFS is suppressed when the soliton spectrum approaches the ZDP. The suppression is due to a transfer of the substantial amount of energy from the soliton to radiation.

(ii) For $\bar{\beta}_{4,th1}\lessgtr\bar{\beta}_4<\bar{\beta}_{4,th2}<0$ and $\bar{\beta}_3<0$ (part of region 2 and region 3 in Fig. 1), there are two anomalous GVD regions separated by the normal GVD region. Both ZDPs are on the left-hand side of the soliton frequency. Then, the soliton center frequency can switch from one anomalous GVD region to the other, resulting in the soliton spectral tunneling [13,14]. The mechanism of the tunneling is the phase-matching of the soliton with a frequency in the different anomalous GVD region. The tunneling can be accompanied also by effective generation of linear waves due to the four-wave mixing.

(iii) For $\bar{\beta}_{4,th2}<\bar{\beta}_4<0$ and $\bar{\beta}_3<0$ (region 4 in Fig. 1), GVD is anomalous for all frequencies. In this case, there is a smooth variation of ω_s with little radiation.

(iv) For $\bar{\beta}_4<0$ and $\bar{\beta}_3>0$ (regions 6, 7, and 8 in Fig. 1), both ZDPs are on the right-hand side from the soliton frequency. The soliton parameters change slowly following the GVD.

Regimes (i) and (iv) can occur when only cubic dispersion is included, while regimes (ii) and (iii) requires the presence of quartic or higher dispersion. When the carrier frequency differs from the reference frequency, or $\omega_s(0)\neq 0$, the dynamics is similar to one of that listed above with the same relative positions of $\omega_s(0)$ and the ZDPs.

Numerical simulations of Eq. (1) also indicate that the effective energy transfer to the resonance frequency occurs when the pulse parameters differ significantly from the parameters of the fundamental soliton at a given frequency. In the presence of the SFS, this means that the center frequency ω_s and, therefore, $\hat{\beta}_2$ vary so fast that the pulse cannot adjust its form to satisfy the fundamental soliton condition $A\tau=(-\hat{\beta}_2/\gamma)^{1/2}$. One can say that the soliton dynamics is not adiabatic at this stage. Another inference from this observation is that energy transfer can take place even without the Raman effect if the initial pulse is far from the fundamental soliton.

One can generalize the dynamics to an arbitrary GVD dependence (not restricted to the CD and QD terms). To the lowest approximation the soliton width follows the variation of $\hat{\beta}_2=\beta_2(\omega_s)$ so that $\tau\approx -2\hat{\beta}_2/(\gamma Q)$. The frequency shift is described by Eq. (5). These two equations for τ and ω_s and the phase-matching condition (14) are sufficient for understanding the soliton dynamics for a more general dependence of GVD.

In conclusion, our study shows that the soliton SFS can be manipulated effectively by a proper choice of dispersion. We derived approximate equations that describe the soliton SFS in the presence of CD and QD. These equations can be used for estimate of the threshold propagation distance when the soliton starts to transfer appreciable amount of energy to the phase matched frequency. We demonstrated that the soliton spectral tunneling occurs due to the phase matching between frequencies in two different regions with anomalous GVD. The systems with several ZDPs can be useful for frequency conversion, four-wave mixing, and supercontinuum generation.

ACKNOWLEDGMENTS

This work was supported by the Australian Research Council under the ARC Centres of Excellence program. We thank Professor John Dudley for sending us a copy of Ref. [13].

APPENDIX: PERTURBATION EQUATIONS

The generalized nonlinear Schrödinger equation is written as

$$i\psi_z-\frac{\bar{\beta}_2}{2}\psi_{tt}+\gamma|\psi|^2\psi=R[\psi], \tag{A1}$$

where $\bar{\beta}_2$ and γ are constant and $R[\psi]$ is the perturbation. We take a solution of Eq. (A1) in the following form:

$$\psi(t,z)=A(z)F(y)\exp(i\theta), \tag{A2}$$

where $y=[t-t_c(z)]/\tau(z)$ and $\theta=-\omega_s(z)\tau(z)y+\mu(z)\tau^2(z)y^2$. If $F(y)$ is a real *symmetric* function of y, then the following dynamical system for the soliton parameters can be obtained from the invariants of Eq. (A1) and their moments [16] (see also [18]):

$$Q_z=2A\tau\int_{-\infty}^{\infty}F\,\mathrm{Im}[P]dy,$$

$$\omega_{s,z}=-\frac{2A}{Q}\int_{-\infty}^{\infty}F_y\,\mathrm{Re}[P]dy-\frac{4A\tau^2\mu}{Q}\int_{-\infty}^{\infty}yF\,\mathrm{Im}[P]dy,$$

$$\tau_z=-2\bar{\beta}_2\mu\tau+\frac{a_1}{a_2}\frac{A\tau^2}{Q}\int_{-\infty}^{\infty}y^2F\,\mathrm{Im}[P]dy-\frac{A\tau^2}{Q}\int_{-\infty}^{\infty}F\,\mathrm{Im}[P]dy,$$

$$\mu_z=-\frac{\bar{\beta}_2}{2a_2}\frac{1}{\tau^4}\int_{-\infty}^{\infty}(F_y)^2dy+2\bar{\beta}_2\mu^2-\frac{\gamma}{4a_2}\frac{A^2}{\tau^2}\int_{-\infty}^{\infty}F^4dy+\frac{1}{2a_2A\tau^2}\int_{-\infty}^{\infty}(2yF_y+F)\mathrm{Re}[P]dy,$$

$$t_{c,z} = \bar{\beta}_2 \omega_s + \frac{2A\tau^2}{Q} \int_{-\infty}^{\infty} yF \,\mathrm{Im}[P] dy, \tag{A3}$$

where $Q = a_1 A^2 \tau$, $P = R[\psi]\exp(-i\theta)$, and

$$a_1 = \int_{-\infty}^{\infty} F^2 dy, \quad a_2 = \int_{-\infty}^{\infty} y^2 F^2 dy. \tag{A4}$$

A particular case of the system (A3) for $F(y) = \mathrm{sech}(y)$ is presented in Ref. [16]. When

$$R[\psi] = i\frac{\bar{\beta}_3}{6}\frac{\partial^3 \psi}{\partial t^3} - \frac{\bar{\beta}_4}{24}\frac{\partial^4 \psi}{\partial t^4} + \gamma T_R \psi \frac{\partial |\psi|^2}{\partial t},$$

the set of equation (A3) gives Eqs. (4)–(8).

[1] R. H. Stolen and E. P. Ippen, Appl. Phys. Lett. **22**, 276 (1973).
[2] F. M. Mitschke and L. F. Mollenauer, Opt. Lett. **11**, 659 (1986).
[3] J. P. Gordon, Opt. Lett. **11**, 662 (1986).
[4] *The Supercontinuum Laser Source*, edited by R. R. Alfano (Springer, New York, 2006).
[5] J. M. Dudley, G. Genty, and S. Coen, Rev. Mod. Phys. **78**, 1135 (2006).
[6] D. V. Skryabin, F. Luan, J. C. Knight, and P. St. J. Russell, Science **301**, 1705 (2003).
[7] F. Biancalana, D. V. Skryabin, and A. V. Yulin, Phys. Rev. E **70**, 016615 (2004).
[8] E. N. Tsoy and C. M. de Sterke, J. Opt. Soc. Am. B **23**, 2425 (2006).
[9] A. Ferrando, E. Silvestre, J. J. Miret, and P. Andres, Opt. Lett. **25**, 790 (2000).
[10] T.-L. Wu and C.-H. Chao, J. Lightwave Technol. **23**, 2055 (2005).
[11] E. Silvestre, T. Pinheiro-Ortega, P. Andres, J. J. Miret, and A. Coves, Opt. Lett. **31**, 1190 (2006).
[12] K. M. Gundu, M. Kolesik, J. V. Moloney, and K. S. Lee, Opt. Express **14**, 6870 (2006).
[13] B. Kibler, P.-A. Lacourt, F. Courvoisier, and J. M. Dudley, Electron. Lett. (to be published).
[14] V. N. Serkin, V. A. Vysloukh, and J. R. Taylor, Electron. Lett. **29**, 12 (1993).
[15] G. P. Agrawal, *Nonlinear Fiber Optics* (Academic Press, San Diego, 1995).
[16] A. I. Maimistov, J. Exp. Theor. Phys. **77**, 727 (1993).
[17] N. Akhmediev and M. Karlsson, Phys. Rev. A **51**, 2602 (1995).
[18] E. N. Tsoy, A. Ankiewicz, and N. Akhmediev, Phys. Rev. E **73**, 036621 (2006).